Available online at www.sciencedirect.com
ScienceDirect
Ceramics International 37 (2011) 2763–2779
CERAMICS INTERNATIONAL
www.elsevier.com/locate/ceramint

Photostimulated optical effects and some related features of CuO mixed Li_2O–Nb_2O_5–ZrO_2–SiO_2 glass ceramics

T. Srikumar [a], I.V. Kityk [b], Ch. Srinivasa Rao [a], Y. Gandhi [a], M. Piasecki [c], P. Bragiel [c], V. Ravi Kumar [a], N. Veeraiah [a,*]

[a] Department of Physics, Acharya Nagarjuna University – Nuzvid Campus, Nuzvid 521 201, A.P., India
[b] Electrical Engineering Department, Technical University of Czestochowa, Aleja Armii Krajowej 17/19, PL-42-201 Czestochowa, Poland
[c] Institute of Physics, J Dlugosz University Czestochowa, Aleja Armii Krajowej 13/15, 42-200 Czestochowa, Poland

Received 25 March 2011; accepted 18 April 2011
Available online 25 April 2011

Abstract

We have synthesized Li_2O–Nb_2O_5–ZrO_2–SiO_2 glasses and subsequently crystallized them with different CuO contents (0–0.3 mol% in the steps of 0.05) as nucleating agents and characterized them by XRD, SEM and DSC. We have also studied IR, Raman, ESR, optical absorption photoluminescence and dielectric properties to explore the influence of copper valance states and their coordination with oxygen on structural and optoelectronic aspects of the samples. These studies have indicated that there is a possibility for the copper ions to exist in Cu^{+} and Cu^{3+} states (in addition to Cu^{2+} state) in these glass ceramics and participate in the glass network forming. Finally, we have undertaken photoinduced second harmonic generation studies (after the samples were dc field treated at elevated temperatures) with 10 ns Er:glass laser (of wavelength 1540 nm with power densities up to 1.5 GW/cm^2) to examine the suitability of these materials for optically operated devices. The analysis of the results of non-linear optical studies has shown that 0.2 mol% of CuO is the optimal concentration for getting the highest values of second order susceptibility coefficients.

Keywords: B. Spectroscopy; C. Dielectric properties; D. Glass ceramics; D. Silicate

1. Introduction

Niobium silicate glasses and glass ceramics mixed with transition metal ions are well known due to their electro chromic and non-linear optical properties [1–4]. The addition of ZrO_2 to these glasses makes them to be more electrical, chemical and thermal resistant; the presence of zirconium oxide in oxide glasses also causes to increase the mechanical strength and is found to widen the range of transparency (300 nm to 8 μm) of the glasses [5–7]. In view of these qualities, the ZrO_2 mixed niobium silicate glasses are expected to be useful as optical filters, laser mirrors, and alternative gate dielectrics in microelectronics and in a number of nonlinear devices [8,9].

Partial crystallization of the glasses is expected to have profound influence on several physical properties viz., optical, mechanical, electrical, thermal and chemical durability of the material. Recently, transparent crystallized glasses, i.e., composites of crystalline and glassy phases, consisting of nonlinear optical or ferroelectric crystals have received much attention and there have been many reports on the fabrication and characterization of such transparent crystallized glasses [10]. Transparency of glass ceramics can be retained by controlling the crystallization of a glass precursor with appropriate chemical compositions and appropriate nucleating agent. The general conditions for the retention of transparency of glass even after the crystallization include small refractive index difference between the crystalline and residual glass phases, a small birefringence of the crystallites and smaller wavelength of the incident light when compared with the size of crystallites. Investigations along these lines have been carried out on several glass systems including some silicate, fluoride or oxyfluoride matrices, polymers and thin films [11–15].

Transition metal ions are generally being used as crystal stimulators for controlled crystallization processes, giving rise

* Corresponding author. Tel.: +91 8656 235551; fax: +91 8656 235551.
E-mail address: nvr8@rediffmail.com (N. Veeraiah).

0272-8842/$36.00
doi:10.1016/j.ceramint.2011.04.031

to enormous numbers of nucleation centers in the original glass. Among various transition metal ions, copper ion is a very interesting ion to probe in the glass ceramic material. In the silicate glass matrices this ion is expected to exist as metallic Cu, cuprous Cu^{+}, or cupric Cu^{2+} ions as per the following redox reaction

$$4Cu^{2+} + 2O_2{}^{-} \leftrightarrow 4Cu^{+} + O_2$$

It is known that the valence state in copper affects not only optical, chemical, electrical and mechanical properties but also the glass-forming ability of the system [16,17]. Due to the crystallization, there is a possibility for the formation of copper nanoclusters in glasses; such nano crystals are expected to exhibit absorption bands at characteristic surface plasma resonance in the visible region and optical nonlinearity [18–20]. In view of these qualities, the glass ceramics containing copper ions in different oxidation states are highly useful for consideration of the materials to use in electrical memory switching devices. There are also reports suggesting that copper ions in some glass ceramics containing alkali ions like lithium do exist in Cu^{3+} state and form $LiCuO_2$ crystal phases with Li-layered structures. Li–Cu–O containing systems have attracted great interest as cathode materials for advanced lithium ion batteries [21].

Further, thermally poled silica based glasses and glass ceramics under electrical fields are the materials of choice for applications in optoelectronics because of their excellent optical properties; recently for some of the silicate based glasses, the value of $\chi^{(2)}$ is reported to be ~0.30 pm/V [22]. For applications like modulators, routers or switches, the amplitude of the electric field E_{dc} recorded in the material has to be strong and stable at the place of the optical waveguides. The stability of the electric field in the poled glasses is, thus, an important factor in determining the nonlinear optical properties produced during the poling process.

In the present investigation we have synthesized Li_2O–Nb_2O_5–ZrO_2–SiO_2 glasses, crystallized them with different concentrations of CuO as nucleating agents and characterized them by a variety of techniques viz., XRD, SEM and DSC. Later, we have studied IR, Raman, ESR, optical absorption photoluminescence and dielectric properties with a view to have some understanding over the influence of copper valance states and their coordination with oxygen on structural aspects of the samples. Finally, we have undertaken photoinduced second order susceptibility studies (after the samples were dc field treated at elevated temperatures) to examine the suitability of these materials for optically operated devices.

2. Experimental

The detailed compositions of the glasses used in the present study are as follows:

C_0: $30.00Li_2O-10Nb_2O_5-5ZrO_2-55SiO_2$

C_5: $29.95Li_2O-10Nb_2O_5-5ZrO_2-55SiO_2$: 0.05CuO

C_{10}: $29.90Li_2O-10Nb_2O_5-5ZrO_2-55SiO_2$: 0.10CuO

C_{15}: $29.85Li_2O-10Nb_2O_5-5ZrO_2-55SiO_2$: 0.15CuO

C_{20}: $29.80Li_2O-10Nb_2O_5-5ZrO_2-55SiO_2$: 0.20CuO

C_{25}: $29.75Li_2O-10Nb_2O_5-5ZrO_2-55SiO_2$: 0.25CuO

C_{30}: $29.70Li_2O-10Nb_2O_5-5ZrO_2-55SiO_2$: 0.30CuO

Analytical grade reagents of Li_2CO_3, Nb_2O_5, ZrO_2, SiO_2 and CuO powders in appropriate amounts (all in mol%) were thoroughly mixed in an agate mortar and melted in a platinum crucible in the temperature range of 1450–1500 °C in an automatic temperature controlled furnace for about 30 min. The resultant bubble free melt was then poured in a brass mould and subsequently annealed at 400 °C. For the crystallization, the glass specimens were first heated up to crystallization temperature 900–950 °C (identified from DSC traces) at the rate of 3 °C/min and then were held at 900 °C for 72 h; samples were cooled slowly (for about 3 h) to the off-set temperature of the crystallization peak (to avoid cracks, voids due to subsequent sudden cooling) and then chilled in air to room temperature.

The samples prepared were mechanically ground and polished to a mirror finish with cerium oxide powder; the final dimensions of the samples used for the measurements are about 1 cm × 1 cm × 0.2 cm. Scanning electron microscopy studies were carried out on these samples to observe the crystallinity using HITACHI S-3400N Scanning Electron Microscope. The crystalline phases in the heat treated samples were identified using Rigaku D/Max ULTIMA III X-ray diffractometer with CuK_α radiation. Differential thermal analysis was carried out by Netzsch Simultaneous DSC/TG Thermal Analyzer STA409C with 32-bit controller to determine the glass transition temperature and crystalline peaks. High temperature furnace together with a sample carrier suitable for C_p measurements and Al_2O_3 crucibles was used. Apparatus was calibrated both for temperature and for sensitivity with melting temperatures and melting enthalpies of the pure metals: Ga, In, Sn, Zn, Al, Ag, and Au. All the recordings were carried out in argon (5 N pure) atmosphere to prevent samples from oxidation. Heating rate was 10 °C/min in the temperature range 32–1300 °C.

The density of the glasses was determined to an accuracy of (±0.0001) by the standard principle of Archimedes' using o-xylene (99.99% pure) as the buoyant liquid. The mass of the samples was measured to an accuracy of 0.1 mg using Ohaus digital balance Model AR2140 for evaluating the density. The refractive index (n) of the samples was measured at $\lambda = 589.3$ nm using Abbe refractometer with monobromo naphthalene as the contact layer between the glass and the refractometer prism to an accuracy of 0.001. Infrared transmission spectra were recorded on a JASCO-FT/IR-5300 spectrophotometer that can record spectrum up to a resolution of 0.1 cm^{-1} in the spectral range 400–2000 cm^{-1} using potassium bromide pellets (300 mg) containing pulverized sample (1.5 mg). These pellets were pressed in a vacuum die at ~680 MPa. The Raman spectra were recorded with an NIR excitation line (1064 nm) using a Bio-Rad spectrometer FTS

175C equipped with an FT Raman supplementary accessory working in a back-scattering geometry system. The ESR spectra of the fine powders of the samples were recorded at room temperature on E11Z Varian X-band (ν = 9.5 GHz) ESR spectrometer. The optical absorption spectra of the glasses were recorded to a resolution of 0.1 nm at room temperature in the spectral wavelength range covering 300–1000 nm using JASCO Model V-670 UV–vis–NIR spectrophotometer. The luminescence spectra of the samples were recorded at room temperature on Photon Technology International fluorescence spectrophotometer. This instrument contains auto calibrated quadrascopic monochrometer for wavelength selection and quadracentric sample compartment.

The method of measuring second order non linear susceptibility consists of recording the power of the second-harmonic wave generated within the poled sample as a function of applied dc field at elevated temperatures. The beam of an Er glass laser of wavelength 1540 nm was focused onto the poled region of the sample. The non linear optical effects (controlled by the output of SHG) were recorded after the achievement of maximal poling; the incident beam of the 10 ns Er:glass laser (of wavelength 1540 nm with power densities up to 1.5 GW/cm^2 per pulse and frequency repetition about 10 Hz) was split by beam splitter into two beams: the first one is with a wavelength of 1540 nm and the second one is a doubled frequency beam. For better poling, the samples were heat treated at elevated temperature and at different dc-fields. After 3–4 min of such treatment the signal of the SHG started procuring intensity and got saturated within several minutes and finally the output SHG was recorded. A brief sketch of the experimental setup used for these measurements is shown in Fig. 1. Other details of these measurements were reported in an earlier paper from our group [23].

Thin coating of silver paint was applied on either side of the samples to serve as electrode for taking dielectric measurements. The dielectric measurements were carried out on LCR Meter (Hewlett-Packard Model-4263 B) in the frequency range 10^2–10^5 Hz and in the temperature range 30–300 °C. The accuracy in the measurement of dielectric constant is ∼0.001 and that of loss is $\sim 10^{-4}$.

3. Results

From the measured values of the density and average molecular weight M of the samples, various other physical parameters such as copper ion concentration N_i, mean copper ion separation R_i, polaron radius R_p in Li_2O–Nb_2O_5–ZrO_2–SiO_2:CuO ceramic samples are computed and presented in Table 1. The density of the samples is observed to increase slightly with the concentration of CuO.

The scanning microscopy pictures of some of the samples are shown in Fig. 2. The pictures clearly indicate that the samples contain well defined, randomly distributed crystals of different sizes (varying from 100 to 500 nm) ingrained in glassy matrix. The residual glass phase is acting as an interconnecting zone among the crystallized areas making the samples free of voids and cracks. The pictures further indicate a gradual increase in the volume fraction of crystallites in the samples with increasing concentration of CuO. Thus, from these pictures it can also be concluded that CuO enhanced the phase separation tendency of various crystalline phases. The SEM pictures of pre-heated samples exhibited virtually no crystallinity. For the sake of comparison the SEM picture of one of the pre-heated samples is presented in Fig. 2.

X-ray diffraction patterns for the Li_2O–Nb_2O_5–ZrO_2–SiO_2 glass ceramic doped with 0.2 mol% of CuO are shown in Fig. 3(a). The patterns exhibited peaks due to a variety of crystal phases; some of them are Li_6CuO_4, $CuSiO_3$, $Li_6Si_2O_7$, $Li_2Si_3O_5$, Li_8SiO_6, $Li_2Si_2O_5$, Li_4SiO_4, Li_2SiO_3, $Li_2Si_3O_7$, Li_3NbO_4, $Li_{10}Nb_2O_{10}$, $Li_8Nb_2O_9$, $LiNbO_2$, $Li_{12}Nb_{17}O_{33}$, $LiNb_3O_8$, $Li_2Nb_{32}O_{81}$, Li_7NbO_6, Li NbO_3, $ZrNb_2O_7$, $ZrNb_{10}O_{27}$, $ZrNb_{14}O_{37}$, $Zr_6Nb_2O_{17}$, $CuNb_2O_6$, $CuNbO_3$ and $Cu_3Nb_2O_8$; the details of JCPDS card numbers for these crystalline phases can be found in Ref. [24]. The XRD patterns

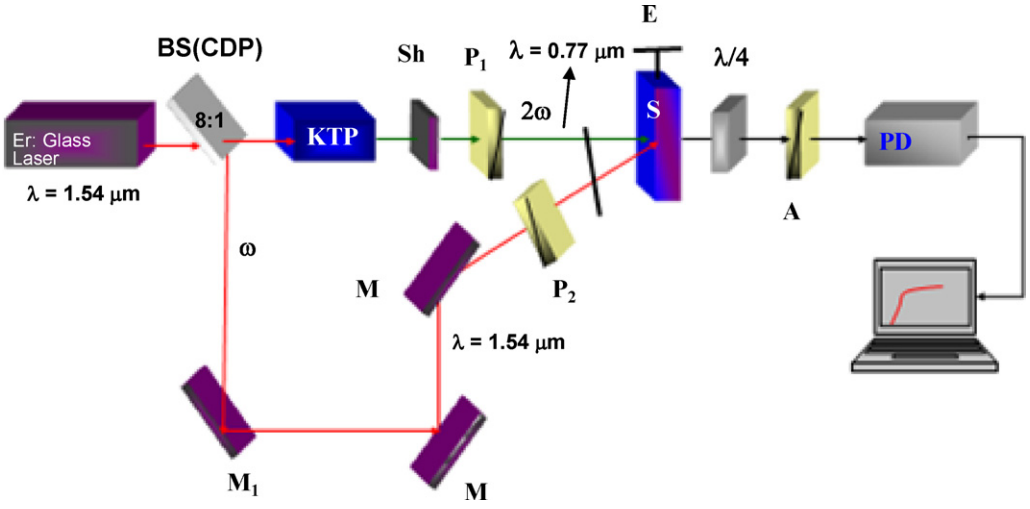

Fig. 1. Principal set-up used for the measurement of second order susceptibility. The diameters of the beams at the focal point were about 260 and 170 mm for the fundamental and doubled harmonic frequencies respectively. The typical laser power densities at the waist were $I_\omega \sim 1.5$ GW/cm^2 and $I_{2\omega} \sim 0.2$ GW/cm^2. Pulse duration is 10 ns and repetition frequency is 10. The sensitivity threshold of the measuring system was about 1 mW/pulse.

Table 1
Physical parameters of Li_2O–Nb_2O_5–ZrO_2–SiO_2:CuO glass ceramic samples.

Sample	Density (g/cm^3)	Cu ion conc. N_i ($\times 10^{20}$/cm^3)	Inter ionic distance R_i (Å)	Polaron radius R_p (Å)	Field strength (10^{15}, cm^{-2})	Molar volume (cm^3/mol)	Electronic polarizability (10^{-22})	Refractive index (n)
C_0	3.0966	0	0	0	0	24.14	4.40	1.781
C_5	3.0979	0.01	9.30	3.75	1.42	24.14	4.40	1.783
C_{10}	3.0993	0.25	7.37	2.97	2.27	24.13	4.41	1.785
C_{15}	3.1011	0.37	6.44	2.59	2.97	24.13	4.40	1.786
C_{20}	3.1033	0.50	5.85	2.36	3.60	24.12	4.41	1.788
C_{25}	3.1053	0.62	5.43	2.19	4.18	24.11	4.42	1.789
C_{30}	3.1068	0.75	5.11	2.06	4.72	24.11	4.42	1. 790

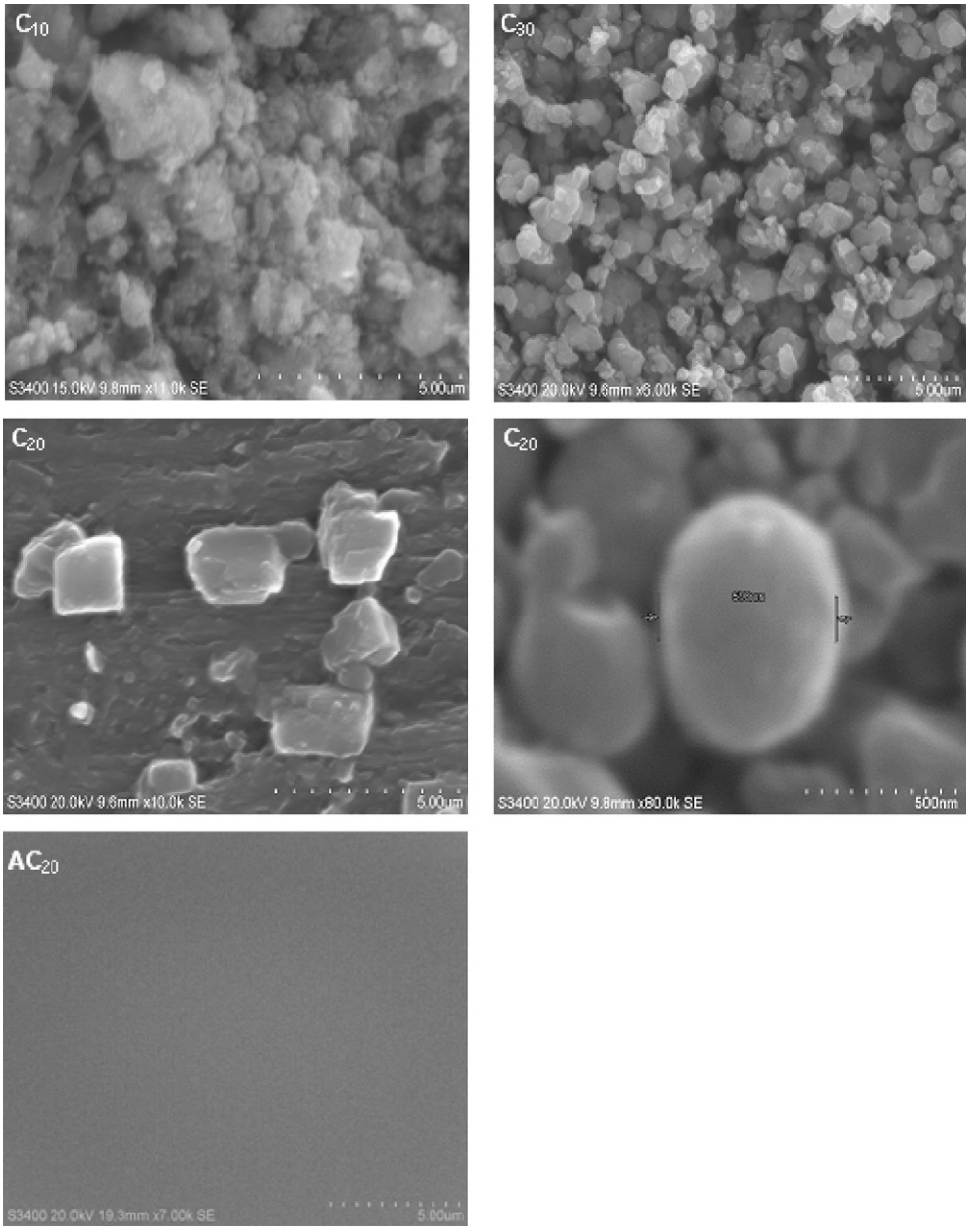

Fig. 2. SEM photographs of some of the crystallized samples of Li_2O–Nb_2O_5–ZrO_2–SiO_2 doped with different concentrations of CuO. For the sample C20 SEM photographs with two different magnifications are presented. The figure also contains SEM photographs of one of the (AC_{20}) pre-crystallized samples.

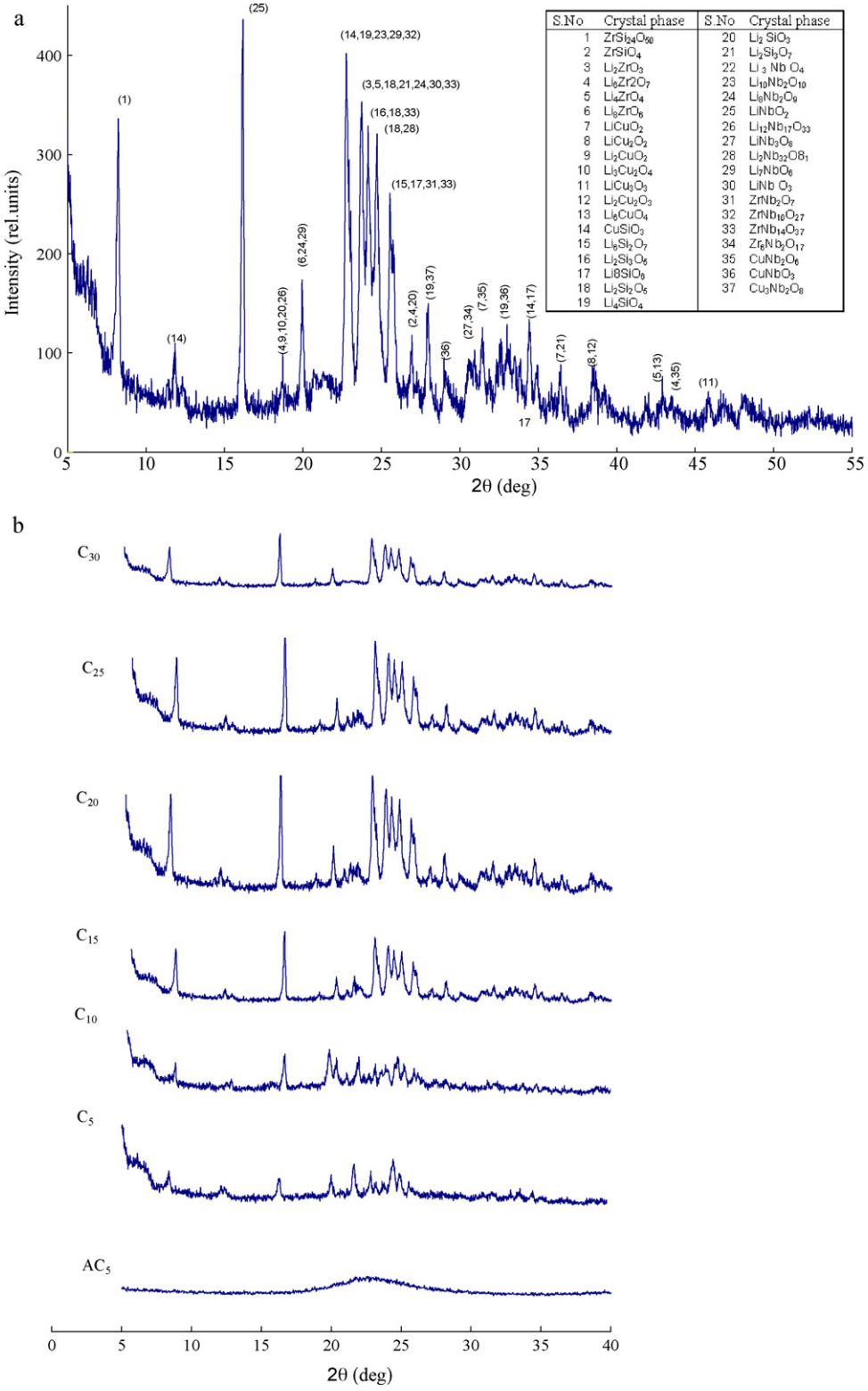

Fig. 3. (a) XRD pattern of Li_2O–Nb_2O_5–ZrO_2–SiO_2 glass ceramics doped with 0.2 mol% of CuO showing different possible crystal phases. (b) XRD pattern of Li_2O–Nb_2O_5–ZrO_2–SiO_2 glass ceramics doped with different concentrations of CuO. For the sake of comparison XRD pattern of one of the pre-crystallized samples (AC_5) is also included.

for all the crystallized glasses are shown in Fig. 3(b). Most interestingly we have also observed a diffraction peak with a significant intensity and full width at half maximum due to LiCuO crystal phase at about $2\theta = 25.59^\circ$. The presence of such phase clearly suggests that a fraction of the copper ions do exist in Cu^+ state. However, as the concentration of CuO increased, no considerable hike in the intensity of this peak is observed. Another interesting feature of XRD pattern is, the presence of

clear peaks at $2\theta = 31.34^\circ$ and 36.59° corresponding to $LiCuO_2$ orthorhombic crystal phases; this observation points out that there is a possibility for the copper ions to exist in Cu^{3+} state and participate in the network forming with square planar CuO_4 structural units connected linearly along the *c*-axis as shown in Fig. 4 [25]. It may be noted here that the XRD patterns of pre-heated samples have not exhibited any sharp peaks (Fig. 3(b)).

In Fig. 5(a) and (b), differential scanning calorimetric (DSC) scans for Li_2O–Nb_2O_5–ZrO_2–SiO_2:CuO glasses and glass-ceramics in the temperature region 300–1500 K are presented. The DSC traces of pre-crystallized samples (Fig. 5(a)) indicated typical glass transitions (T_g) with the inflection point between 817 and 844 K followed by a broad exothermic change due to crystallization. As the concentration of CuO is increased up to 0.2 mol% of CuO, a slight decrease in the glass transition temperature and the parameter T_c–T_g is observed and a slight increasing trend of these parameters is observed for the samples C_{25} and C_{30} (Table 2a).

For the crystallized glasses, a weak endothermic affect (due to glass transition) at about 825 K with decreasing trend in ΔC_p (Fig. 5(b) and Table 2b) with the concentration of CuO is visualized. At about 1250 K, the DSC thermograms of each glass ceramic exhibited well-defined exothermic effects with multiple steps of crystallization temperatures connected with different crystalline phases; the auxiliary peaks appear to be weak and spread over a region of approximately 100 K. The variation of enthalpy associated with the primary crystallization peak with the concentration of crystallizing agent is shown as the inset (i) in Fig. 5(b). The enthalpy is observed to be the maximum for the samples crystallized with 0.20 mol% of CuO. To observe the mass change effects during heating process, we have also recorded thermal gravimetric traces for all the samples; in the inset (ii) of Fig. 5(b), TG traces for two of the samples along with corresponding DSC traces are shown. The analysis up to 1500 K exhibits virtually no change in the mass of the samples.

Fig. 6(a) represents the optical absorption spectra of Li_2O–Nb_2O_5–ZrO_2–SiO_2:CuO glass ceramics recorded at room temperature in the wavelength region 200–1200 nm. The absorption spectra of all the glasses exhibited a broad band with a meta center between 800 and 850 nm. With an increase in the concentration of CuO (at least up to 0.20 mol%), the half width at full maximum and peak height of this broad band is observed to increase. Further, a considerably larger increase in the cut-off wavelength (from 321 to 380 nm) is observed due to increasing concentration of CuO. From the observed absorption edges, we have evaluated the optical band gaps (E_o) of these glasses by drawing Urbach plot between $(\alpha\,\hbar\,\omega)^{1/2}$ and $\hbar\,\omega$ (Fig. 6(b)). The value of E_o is found to decrease with the increase in the content of CuO (inset of Fig. 6(b) and Table 3).

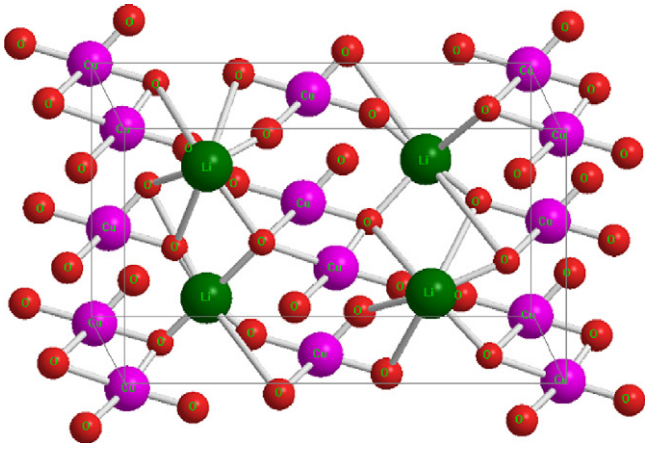

Fig. 4. A possible illustration of $LiCuO_2$ structural unit in which copper ions exist in Cu^{3+} state.

It may be noted here that in the spectra of the pre-crystallized samples (especially for the samples doped with less than 0.2 mol% of CuO) a weak band at about the same wavelength could be visualized. However the optical band gap is found to be considerably higher for the pre-crystallized samples.

Fig. 7 shows the photoluminescence spectra of Li_2O–Nb_2O_5–ZrO_2–SiO_2:CuO glass ceramics recorded at room temperature at the excitation wavelength corresponding to the absorption edge. Emission spectra exhibited emission band in the yellow region centered at about 552 nm and a weak blue emission centered at about 440 nm. As it can be seen from the figure these bands are more intense in the spectra of the samples C_{25} and C_{30}. For the sake of comparison the spectrum of one of the glass samples (AC_5) is also presented in the same figure. The spectrum of the amorphous samples exhibited very feeble kinks at about the same wavelength. It may be noted here that the spectrum of either amorphous or crystallized samples free of CuO does not exhibit any emission bands.

The infrared spectra (Fig. 8) of CuO free Li_2O–Nb_2O_5–ZrO_2–SiO_2 glass ceramics exhibited the following bands [26]:

(i) at 1050 cm^{-1} due to Si–O–Si asymmetric vibrations,
(ii) 800 cm^{-1} due to bending mode of bridging oxygen perpendicular to Si–Si,
(iii) axis within the Si–O–Si plane (symmetrical vibrational band),
(iv) 980 cm^{-1} due to Si–O–Zr linkages,
(v) 850 and 600 cm^{-1} due to Nb=O, Nb–O–Nb stretching vibrations,
(vi) 530 and 700 cm^{-1} due to Zr–O–Zr vibrations of ZrO_4/ν_3-NbO_6 structural units,
(vii) 475 cm^{-1} due to Si–O–Si/O–Si–O bending modes.

As the concentration of CuO is increased, the bands due to asymmetrical vibrations of silicate and other structural units are observed to grow at the expense of symmetrical bands with a slight shift towards lower energies (Table 4). A slight reversal trend in the intensities of these bands could be visualized when the concentration of CuO is raised beyond 0.20 mol%.

The Raman spectra (Fig. 9) of CuO doped glass ceramics have exhibited three prominent bands (Table 5) at about 1053, 810 and 478 cm^{-1} due to symmetrical, asymmetrical and rocking motion of Si–O–Si structural units respectively [27]. As the concentration of CuO is increased all the symmetrical and asymmetrical bands exhibited a behaviour similar to those spectral bands. Additionally, the bands due to distorted NbO_6 structural units

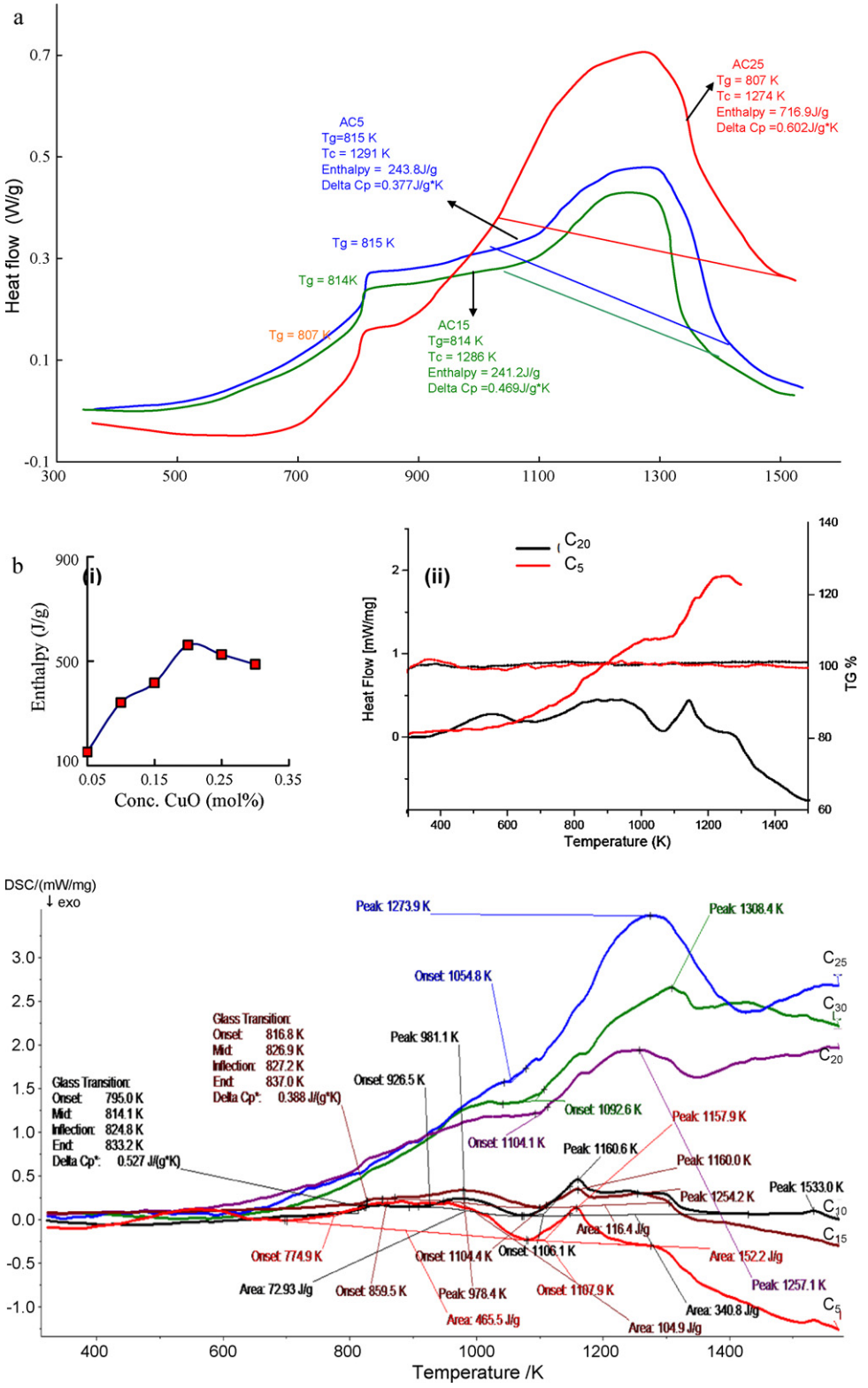

Fig. 5. (a) DSC traces of Li_2O–Nb_2O_5–ZrO_2–SiO_2 glasses doped with different concentrations of CuO. (b) DSC traces of Li_2O–Nb_2O_5–ZrO_2–SiO_2 glass ceramics doped with different concentrations of CuO and inset (i) shows the variation of enthalpy with concentration of CuO. In inset (ii) TG traces for two of the samples along with corresponding DSC traces.

have also been located at about 925 cm^{-1} (highly distorted) and 607 cm^{-1} (less distorted). The significant increase in the intensity of highly distorted band is observed with increasing content of CuO up to 0.20 mol% in the glass matrix.

The patterns of IR and Raman spectra of the amorphous samples remain the same but the variation in the relative intensity of the peaks is noted. The comparison of these spectra with those of crystallized samples indicated that the intensity of

Table 2a
Summary of various DSC traces of Li_2O–Nb_2O_5–ZrO_2–SiO_2 glasses doped with different concentrations of CuO.

Glass	CuO conc. (mol%)	Glass transition temp. (K) (point of inflection)	ΔC_p (J/g K)	Cryst. temp. (peak) (K)	Enthalpy of cryst. (first step) (J/g)	$T_c - T_g$
C_0	0.00	844.6	0.577	1278.9	238.1	434.3
C_5	0.05	824.6	0.377	1286.3	248.3	461.7
C_{10}	0.10	823.3	0.389	1282	247.2	458.7
C_{15}	0.15	822.5	0.411	1280	249.2	457.5
C_{20}	0.20	817.9	0.712	1269.8	826.4	451.9
C_{25}	0.25	822.3	0.602	1274.6	716.9	452.3
C_{30}	0.30	834.0	0.512	1290	354.9	456

Table 2b
Summary of various DSC traces of Li_2O–Nb_2O_5–ZrO_2–SiO_2 glass ceramics doped with different concentrations of CuO.

Glass ceramic	CuO conc. (mol%)	Glass transition temp. (K) (inflection)	ΔC_p (J/g K)	Cryst. temp. onset (K)	Cryst. temp. (peak) (K) first step	Enthalpy of cryst. first step (J/g)
C_5	0.05	825.8	0.528	1107.9	1157.9	152.2
C_{10}	0.10	824.8	0.527	1106.1	1160.6	340.8
C_{15}	0.15	827.2	0.388	1104.4	1160.0	416.4
C_{20}	0.20	828.3	0.141	1096.6	1308.4	561.7
C_{25}	0.25	826.8	0.160	1054.8	1273.9	525.4
C_{30}	0.30	826.1	0.181	1104.1	1257.1	487.9

all asymmetrical bands is considerably lower for the pre-crystallized samples.

The ESR spectra (Fig. 10) of Li_2O–Nb_2O_5–ZrO_2–SiO_2:CuO glass ceramics recorded at room temperature have exhibited a strong asymmetric signal with a hyperfine structure partially resolved at $g_\perp \sim 2.08$ and a shallow quadruplet at about $g_\parallel \sim 2.4$. The components of g are observed to vary considerably with the concentration of CuO (Table 6). The line width of parallel and perpendicular hyperfine peak (of spectra of all the samples) is observed to increase with the order of magnetic quantum number m_1. As the concentration of CuO is increased beyond 0.2 mol%, a considerable decrease in the intensity of the signal is observed. For the pre-crystallized samples the intensity of this signal is found to be comparatively lower (Fig. 10).

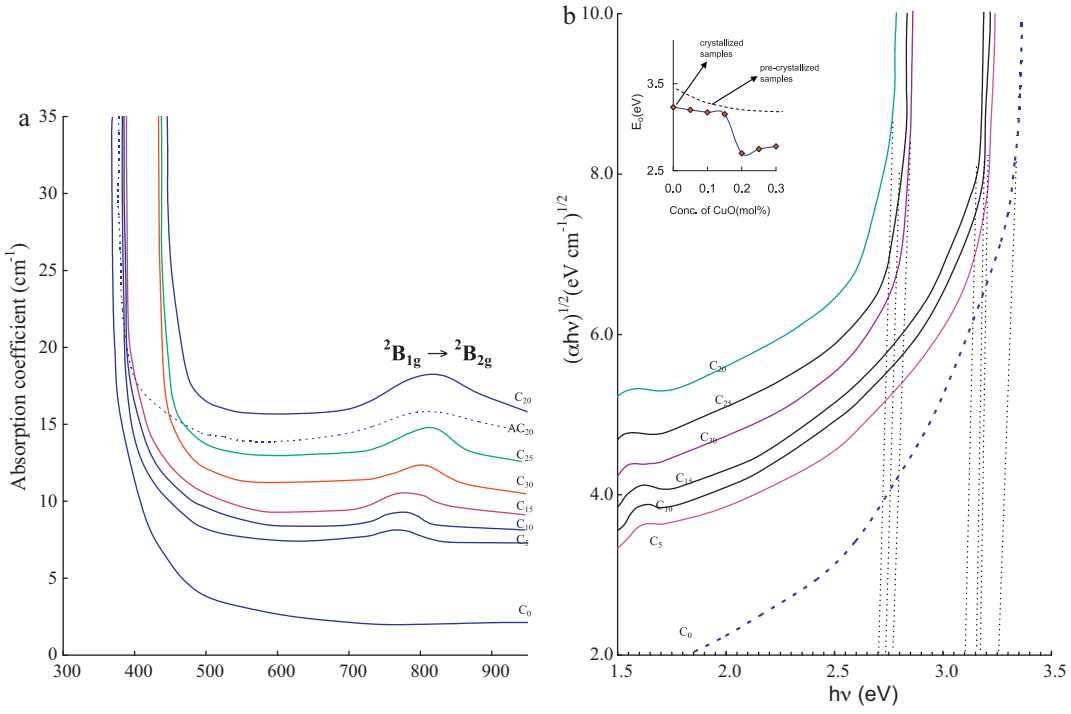

Fig. 6. (a) Optical absorption spectra of Li_2O–Nb_2O_5–ZrO_2–SiO_2 glass ceramics doped with different concentrations of CuO recorded at room temperature and the figure also represents the spectra of pre-crystallized sample AC_{20}. (b) Urbach plots for evaluating the optical band gap of Li_2O–Nb_2O_5–ZrO_2–SiO_2:CuO glass ceramics. Inset represents the variation of optical band gap with the concentrations of CuO for amorphous and glass ceramic samples.

Table 3
Data on optical absorption spectra Li_2O–Nb_2O_5–ZrO_2–SiO_2 glass ceramics doped with different concentrations of CuO.

Glass ceramic	Cut-off wavelength (nm)	Position of $^2B_{1g} \rightarrow {}^2B_{2g}$ band (nm)	E_o (eV)
C_0	380	–	3.23
C_5	385	764	3.20
C_{10}	389	779	3.17
C_{15}	392	802	3.15
C_{20}	448	827	2.70
C_{25}	440	815	2.75
C_{30}	436	806	2.78

Fig. 11(a) represents the comparison plot of second-order susceptibility *vs*. applied dc field at a temperature of 270 °C (by trial and error we have identified this is the optimal temperature for getting the maximal photoinduced second harmonic generation) for the glass ceramic samples; the figure indicates substantial increase of the second-order susceptibility with the increase of the field for all the samples. In the inset of Fig. 11(a), we have plotted the variation of second-order susceptibility with the concentration of the crystallizing agent at the pump power density of 1.2 GW/cm^2 (λ = 1540 nm) measured under the field treatment of 3.5 kV/cm at a temperature of 270 °C; the variation exhibits maximal effect at about 0.2 mol% of CuO and for further increase of CuO content, a considerable decrease of second-order susceptibility could be observed. Fig. 11(b) represents the similar data for some of the amorphous

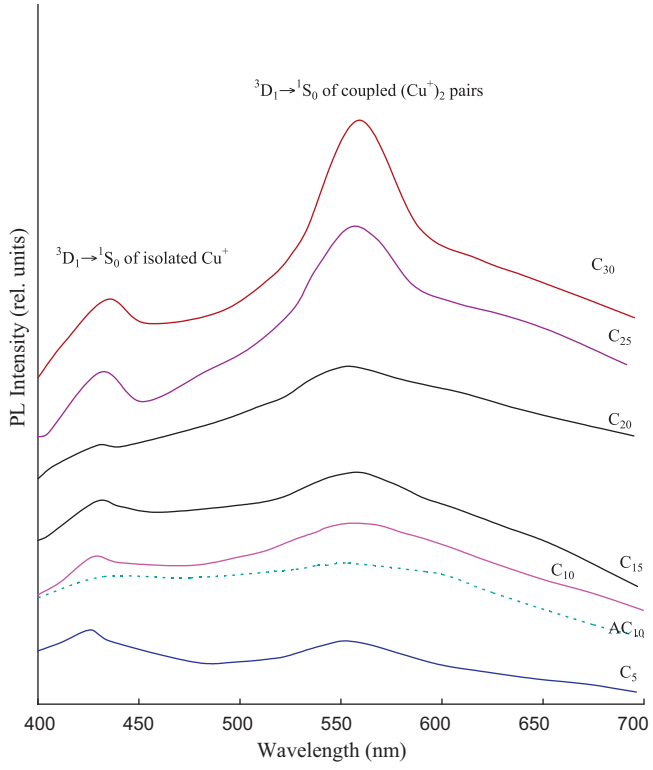

Fig. 7. Photoluminescence spectra of Li_2O–Nb_2O_5–ZrO_2–SiO_2 glass ceramics doped with different concentrations of CuO recorded at room temperature. The figure also contains the PL spectrum of one of the pre-crystallized samples (AC_{10}).

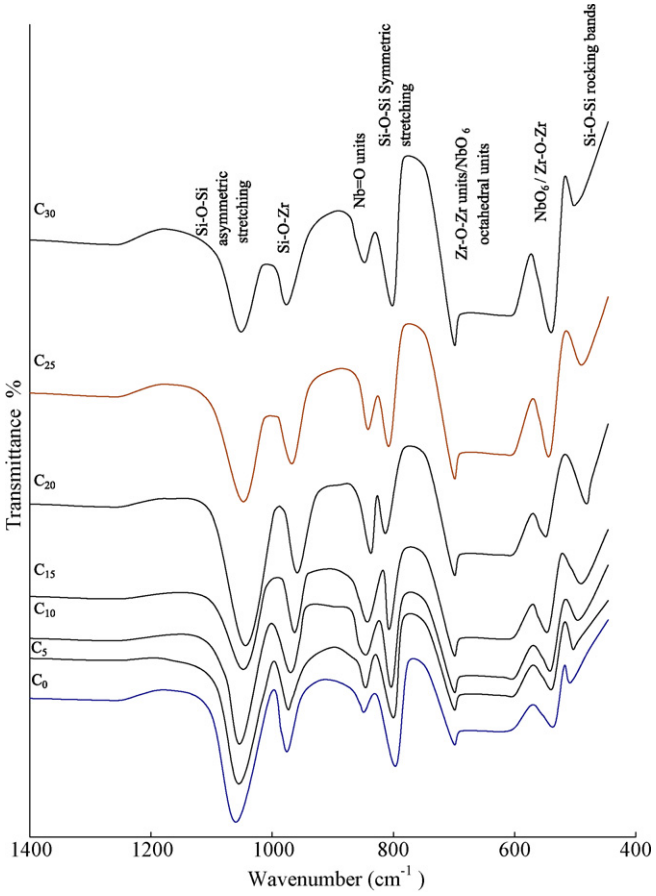

Fig. 8. IR spectra of Li_2O–Nb_2O_5–ZrO_2–SiO_2 glass ceramics doped with different concentrations of CuO.

samples; for these samples the maximal effects were observed at about 320 °C for the same pump density and dc field treatment.

The dielectric constant ε' and loss tan δ at room temperature (≈30 °C) of CuO free Li_2O–Nb_2O_5–ZrO_2–SiO_2 pre-crystallized glasses at 100 kHz are measured to be 6.45 and 0.018 respectively. The temperature dependence of dielectric constant of Li_2O–Nb_2O_5–ZrO_2–SiO_2 glass and glass ceramic samples containing 0.2 mol% of CuO measured at different frequencies is presented in Fig. 12(a). The temperature dependence of tan δ of Li_2O–Nb_2O_5–ZrO_2–SiO_2 glass and glass ceramic samples containing 0.1 mol% of CuO measured at different frequencies is presented in Fig. 12(b). The close look of these figures clearly suggests that the rate of increase of ε' and tan δ with temperature is higher for the glass ceramic samples when compared with that of pre-crystallized glass samples containing the same concentration of CuO at any frequency.

Fig. 13 indicates the variation of ε' with temperature, measured at a frequency of 1 kHz for Li_2O–Nb_2O_5–ZrO_2–SiO_2 glasses and glass ceramics with different concentrations of CuO. Fig. 14 and its inset represent the variation of tan δ with temperature measured at a frequency of 10 kHz for Li_2O–Nb_2O_5–ZrO_2–SiO_2:CuO glass ceramics and glasses. The maximal effects of both dielectric constant and loss with temperature are observed at about 0.2 mol% of CuO.

Table 4
Summary of data on various band positions (cm^{-1}) in IR spectra of Li_2O–Nb_2O_5–ZrO_2–SiO_2:CuO glass ceramics.

Glass ceramic	Si–O–Si asymmetric	Si–O–Si symmetric	Si–O–Si rocking	Zr–O–Zr	Nb═O units	Nb–O–Nb	NbO_6 units	Si–O–Zr
C_0	1059	796	508	701	848	600	533	973
C_5	1055	799	504	701	845	600	537	974
C_{10}	1051	803	497	701	843	600	539	971
C_{15}	1047	807	486	701	841	600	544	963
C_{20}	1043	812	483	701	837	600	546	958
C_{25}	1048	806	490	701	842	600	541	966
C_{30}	1055	800	503	701	847	600	537	974

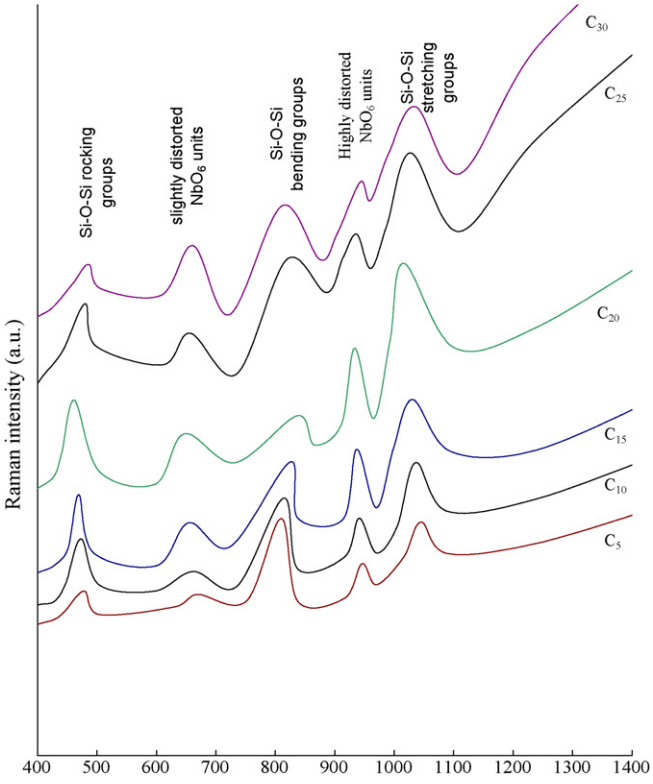

Fig. 9. Raman spectra of Li_2O–Nb_2O_5–ZrO_2–SiO_2 glass ceramics doped with different concentrations of CuO.

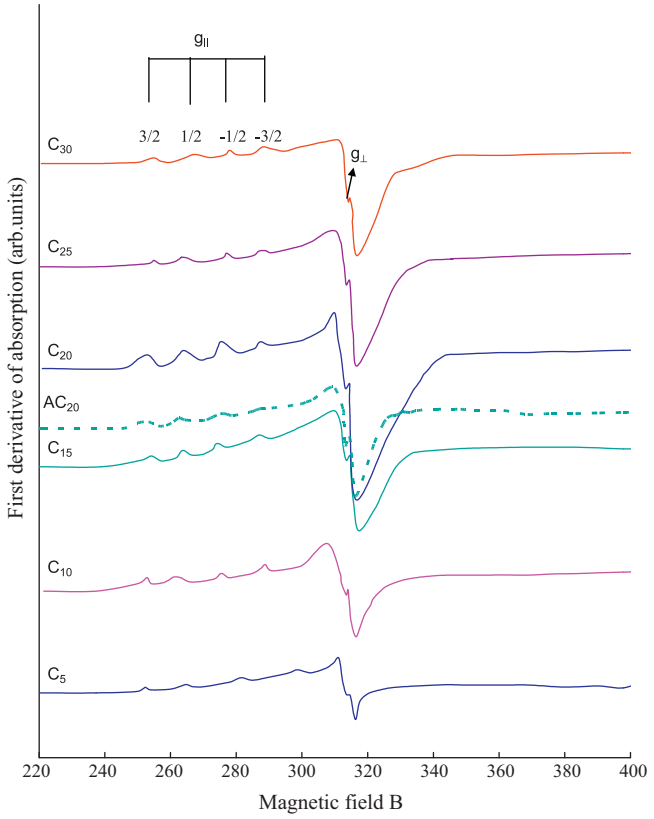

Fig. 10. ESR spectra of Li_2O–Nb_2O_5–ZrO_2–SiO_2:CuO glass ceramics recorded at room temperature. The figure also contains the spectrum of one of the pre-crystallized samples (AC_{20}).

Further, the variation of tan δ with temperature has exhibited distinct maxima; with an increase in frequency the temperature maximum of tan δ shifts towards higher temperatures and with an increase in temperature, the frequency maximum shifts towards higher frequencies, indicating the relaxation character of dielectric losses in these glass ceramics. From these curves, it is also observed that the region of relaxation shifts towards lower temperatures (with broadening of relaxation peaks and increasing value of $(\tan\delta)_{max}$) with an increase in the concentration of the nucleating agent up to 0.2 mol%. The

Table 5
Summary of data on band positions (cm^{-1}) in Raman spectra of Li_2O–Nb_2O_5–ZrO_2–SiO_2 glass ceramics doped with different concentrations of CuO.

Glass	Si–O–Si asymmetric/Si–O–Zr	Si–O–Si symmetric/AlO_4 units	Si–O–Si rocking/AlO_6 units	Slightly distorted NbO_6 units	Highly distorted NbO_6 units
C_5	1045	810	479	668	946
C_{10}	1036	814	473	662	941
C_{15}	1031	825	469	654	937
C_{20}	1016	837	462	647	933
C_{25}	1028	819	480	657	937
C_{30}	1036	811	486	662	945

Table 6
Data on ESR spectra of Li_2O–Nb_2O_5–ZrO_2–SiO_2 glass ceramics doped with different concentrations of CuO.

Sample	$g_{\parallel}$	$g_{\perp}$	α^2	β_1^2
C_5	2.378	2.082	0.729	0.963
C_{10}	2.373	2.082	0.759	0.905
C_{15}	2.370	2.083	0.779	0.870
C_{20}	2.326	2.086	0.856	0.759
C_{25}	2.335	2.084	0.8301	0.827
C_{30}	2.351	2.083	0.806	0.865

effective activation energy W_d for the dipoles evaluated from these plots, is found to be minimum for the glass crystallized with 0.2 mol% of CuO (Table 7).

The ac conductivity σ_{ac} is calculated at different temperatures, using the relation

$$\sigma_{ac} = \omega\varepsilon_o\varepsilon' \tan\delta \quad (1)$$

and the plots of log σ_{ac} against $1/T$ are shown in Fig. 15 for all the glass ceramics at 100 kHz and for the glass samples as inset (a) at the same frequency. From these plots, the activation energy for conduction in the high temperature region over which a near linear dependence of log σ_{ac} with $1/T$ could be observed is evaluated and presented in Table 7; this activation energy is also found to decrease gradually with an increase in the concentration of the crystallizing agent up to 0.2 mol% of CuO (inset (b) of Fig. 15). For the pre-crystallized samples the value of activation energy is found to be considerably higher when compared with corresponding crystallized samples (inset of Fig. 15).

4. Discussion

Among various constituents of Li_2O–Nb_2O_5–ZrO_2–SiO_2:-CuO glass ceramics, SiO_2 participates in the glass network with tetrahedral $[SiO_{4/2}]^0$ units and all the four oxygens in SiO_4 tetrahedral are shared. With the entry of modifiers Li_2O and CuO into Si–O–Si network, the structure gets depolymerized showing the formation of meta, pyro and ortho-silicates in the order: $[SiO_{4/2}]^0$ (Q^4), $[SiO_{3/2}O]^-$ (Q^3), $[SiO_{2/2}O_2]^{2-}$ (Q^2), $[SiO_{1/2}O_3]^{3-}$ (Q^1) and $[SiO_4]^{4-}$ (Q^0) [28]. Nb_2O_5 participates in the glass network with highly distorted and less distorted NbO_6 octahedron. Zirconium ions do participate in the glass network with ZrO_4 structural units and alternate with SiO_4 structural units and also form the linkages of the type Nb–O–Zr, Nb–O–Cu. Lithium ions may modify these linkages with the formation of Nb–O–Li^+, Zr–O–Li^+ and Si–O–Li^+ structures.

Copper ions are expected to exist mainly in Cu^{2+} state in Li_2O–Nb_2O_5–ZrO_2–SiO_2:CuO glass network. However, the oxidation or reduction of copper ions from Cu^{2+} to Cu^{3+} and Cu^+ appears to be possible during melting, annealing and crystallization processes. Cu^{2+} ions occupy octahedral positions whereas Cu^+ and Cu^{3+} ions are expected to occupy tetrahedral positions in the glass network [29–31].

The progressive introduction of crystallizing agent CuO caused a slight increase in the density of the samples. The degree of structural compactness, the modification of the geometrical configuration of the glassy network, the size of the micro-crystals formed, change in the coordination of the glass forming ions and the fluctuations in the dimensions of the interstitial holes might have influenced the density of the glass ceramic material.

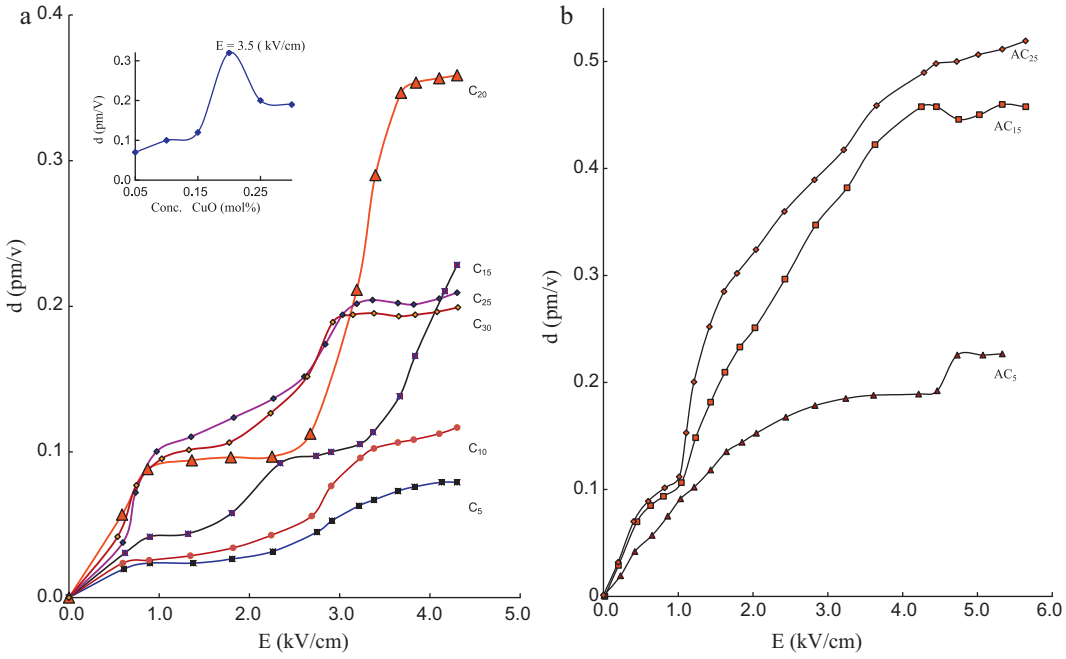

Fig. 11. (a) dc-field dependence of the effective second-order susceptibility for the Li_2O–Nb_2O_5–ZrO_2–SiO_2 crystallized samples doped with different amounts of CuO. A fundamental 20 ns laser Er:glass laser at wavelength 1540 nm was applied. Inset represents the variation of $\chi^{(2)}$ with the concentration of CuO after the dc field treatment (3.5 kV/cm) at a temperature of 270 °C. (b) dc-field dependence of the effective second-order susceptibility for some of the Li_2O–Nb_2O_5–ZrO_2–SiO_2 glass samples doped with different amounts of CuO. A fundamental 20 ns laser Er:glass laser at wavelength 1540 nm was applied at 320 °C.

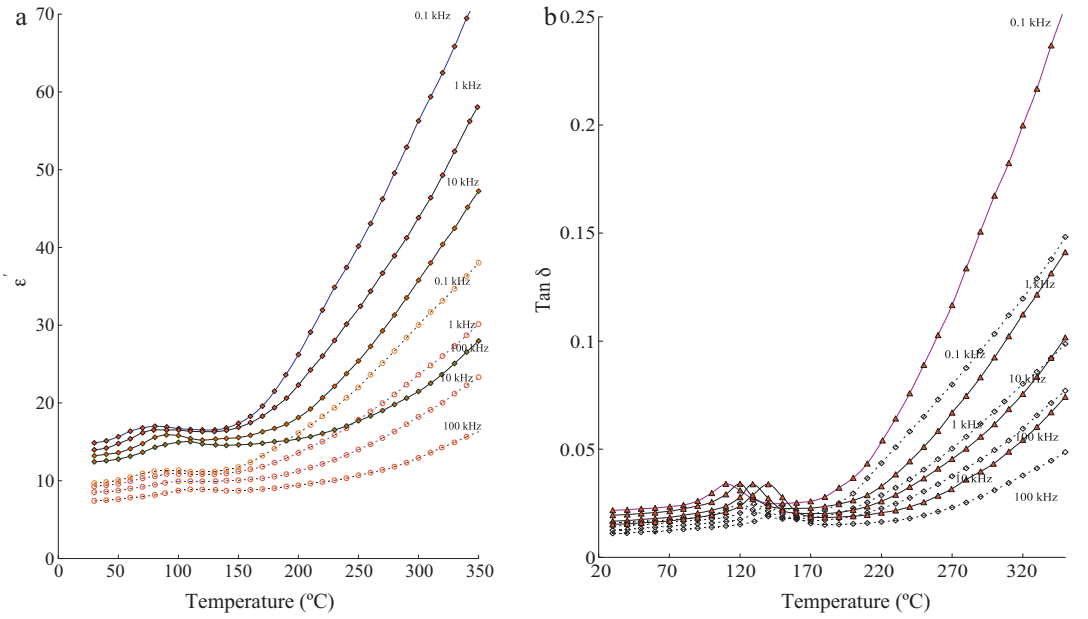

Fig. 12. (a) Variation of dielectric constant of Li_2O–Nb_2O_5–ZrO_2–SiO_2 doped with 0.2 mol% of CuO *i*th temperature at different frequencies before (dashed line) and after crystallization (solid line). (b) Variation of dielectric loss of Li_2O–Nb_2O_5–ZrO_2–SiO_2 doped with 0.1 mol% of CuO with temperature at different frequencies before and after crystallization.

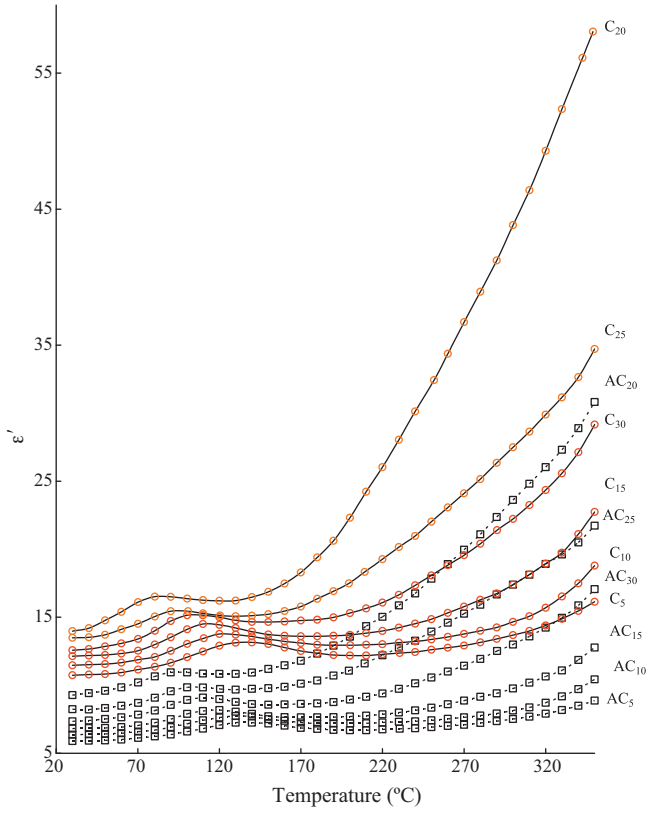

Fig. 13. Variation of dielectric constant of Li_2O–Nb_2O_5–ZrO_2–SiO_2 doped with different concentrations of CuO with temperature at 1 kHz before and after crystallization.

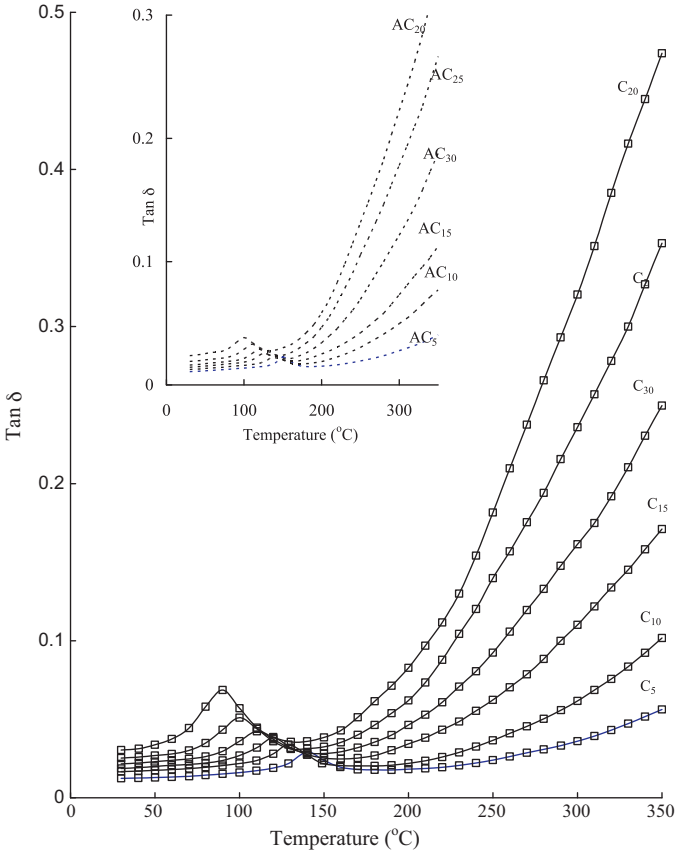

Fig. 14. Variation of dielectric loss of Li_2O–Nb_2O_5–ZrO_2–SiO_2 glasses doped with different concentrations of CuO with temperature at 10 kHz before (inset) and after crystallization.

Table 7
Summary of data on dielectric loss of Li_2O–Nb_2O_5–ZrO_2–SiO_2 glass ceramics doped with different concentrations of CuO.

Glass	A.E. for dipoles (eV)	A.E. for conduction (eV)
C_5	3.42	0.87
C_{10}	3.26	0.74
C_{15}	3.10	0.65
C_{20}	2.65	0.31
C_{25}	2.80	0.40
C_{30}	2.95	0.52

The formation of LiCuO, $LiCuO_2$ crystalline phases detected from the XRD studies along with the other conventional crystalline phases emphasizes that copper ions do exist in Cu^+ and Cu^{3+} state in addition to Cu^{2+} state in these glass ceramics [31]. The relative increase in the intensity of the diffraction peaks due to these crystallites (especially in the pattern of the samples containing CuO greater than 0.2 mol%) indicates increasing proportions of copper ions in these valence states. It was also reported that $LiCuO_2$ crystalline phases are possible both in monoclinic and in orthorhombic structures [31,32]. However, the diffraction peak observed at $2\theta = 31.34^\circ$ points out this crystalline phase possesses orthorhombic structure in these glass ceramics [31].

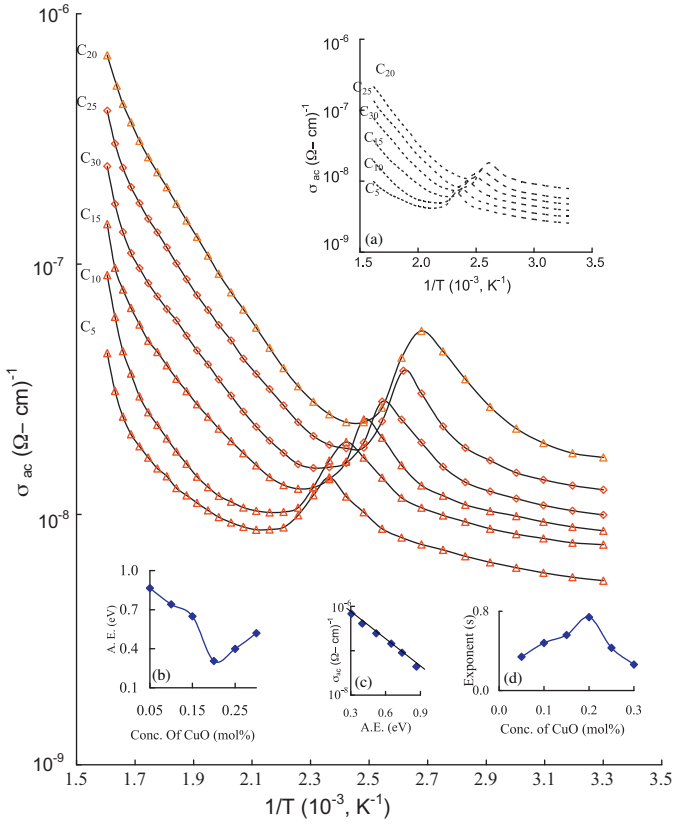

Fig. 15. The variation of ac conductivity of Li_2O–Nb_2O_5–ZrO_2–SiO_2 glasses doped with different concentrations of CuO before (inset a) and after crystallization. Inset b shows the variation of activation energy with concentration of CuO, inset c shows the variation of ac conductivity with activation energy and inset d shows the variation of exponent with the concentration of CuO.

The analysis of the results of DSC studies indicates that with an increase in the concentration of crystallizing agent CuO up to 0.20 mol%, there is a considerable increase in the glass transition temperature T_g. As per empirical relation of Tanaka [33], the relation between T_g and the average coordination number (Z) is represented by

$$\ln T_g \approx 1.6Z + 2.3 \quad (2)$$

This equation clearly suggests that the higher the value of T_g, the higher is the average coordination number; our observations on the glass transition temperature for the present samples are well in accordance with this equation. The appearance of different crystallization temperatures in the DSC pattern obviously suggests the presence of different phases of crystallization in the samples. The crystallization in the glass samples may take place following the surface and bulk nucleations. The general shape of the crystallization peak in DSC curves reflects the variation of enthalpy. The increase in value of enthalpy with increase in the nucleating agent up to 0.2 mol% suggests that the crystallization starts initially inside the material and expands to the surface gradually [34].

The real calorimetric exothermic effects (peaks) caused by crystallization have been suppressed by mutual movement and revolution (aggregation) of metal–oxygen octahedral (endothermic) in the plastic (flexible) phase, at temperature range which appear in the same temperature as the crystallization. This effects decreasing actual enthalpy of crystallization, as indicated by DSC traces due to heat absorption; this is easily confirmed by analysis of DSC traces both heated up to crystallization temperature and glassy sets of samples (Fig. 5(a) and (b)). During this process, the metal-oxygen bond length changes (appear tetrahedral environments of some Cu ions) as manifested by the photoluminescence and optical absorption spectra. Thermo gravimetric analysis confirms high stability and lacks symptom of decomposition up to 1500 K (inset (ii) of Fig. 5(b)) of all the crystallized samples.

The broad absorption band observed in the optical absorption spectra of Li_2O–Nb_2O_5–ZrO_2–SiO_2:CuO glass ceramics is assigned to $^2B_{1g} \rightarrow {}^2B_{2g}$ transition of Cu^{2+} ions [35]. The broadening of this band may be attributed to the super position of three electron transition in d orbitals corresponding to $^2B_{1g} \rightarrow {}^2E_g$, $^2B_{1g} \rightarrow {}^2A_{1g}$ and $^2B_{1g} \rightarrow {}^2B_{2g}$ transitions. Further, the optical activation energy associated with $^2B_{2g} \rightarrow {}^2B_{1g}$ is decreased from 1.62 (sample C_5) to 1.54 eV (sample C_{20}); this is clearly a characteristic signal of inter valence transfer or a polaronic type of absorption. This is possible when the associated electrons are trapped at shallow sites within the main band gap with smaller wave-function radii; in terms of polaronic perception, this kind of situation is only possible if the local potential fluctuation is small as compared to the transfer integral, j. A small overlap between electronic wave functions (corresponding to adjacent sites) due to strong disorder is contributive to polaron formation. So from the polaronic viewpoint, the electron delivered by the impurity atom at the Cu^{2+} site converts this into a lower valence state Cu^+, and at the next stage, the trapped electron at this Cu^+ site is

transferred to the neighboring new Cu^{2+} site by absorbing a photon energy.

Thus the optical absorption in the glass ceramic samples is dominated by polaronic transfer between the Cu^{+} and Cu^{2+} species [36,37]. With the increase in concentration of Cu^{2+} ions in the glass ceramic network, a large number of donor centers are created, and subsequently, the excited states of localized electrons originally trapped on Cu^{+} sites begin to overlap with the empty 3d states on the neighboring Cu^{2+} sites, and as a result, the impurity or polaron band becomes more extended into the main band gap. This new polaronic development might have shifted the absorption edge to the lower energy (Table 3) which leads up to a significant shrinkage in the band gap as the concentration of CuO is increased up to 0.2 mol%. The increasing tendency of optical band gap for the samples C_{25} and C_{30} when compared with that of C_{20} may be attributed to the following reason; in these samples a part of copper ions may exist in Cu^{3+} state that participate in the network forming with linearly connected CuO_4 structural units. Such units increase the rigidity of the glass ceramic network and lead to enhancement of optical band gap for these samples. The IR and Raman spectra suggest less possibility for the presence of such types of structural units in the case of amorphous samples.

In the photoluminescence spectra since no bands were observed in the spectra of CuO free samples, the bands observed are obviously due to the excitation of copper ions. In fact these bands are charge transfer bands of the copper ions; more precisely, the blue kink observed at about 452 nm is due to the $^3D_1 \rightarrow {}^1S_0$ transition of isolated Cu^{+} ions whereas the yellow emission at about 552 nm is due to $^3D_1 \rightarrow {}^1S_0$ transition of $(Cu^{+})_2$ pairs [38,39]. The more intense nature of these bands in the spectra of the C_{25} and C_{30} glass ceramic samples suggests that there is a relatively larger proportion of Cu^{+} ions in these samples.

The observed $g_{\parallel}$ and $g_{\perp}$ values (Table 5) in ESR spectra of CuO mixed Li_2O–Nb_2O_5–ZrO_2–SiO_2 glass ceramics are the characteristics of Cu^{2+} ions coordinated by six ligands from which an octahedron elongated along the z-axis [40]. Because $g_{\parallel} > g_{\perp} > 2.0023$ (g_e), the ground state of the paramagnetic electron is $d_{x^2-y^2}$ orbital ($^2B_{1g}$ state). A comparison of g factors of the studied glass system with other composition of various other oxide glasses reported [41] shows a reasonable agreement.

The ESR and optical absorption spectral data can be correlated to understand the environment of Cu^{2+} ions in Li_2O–Nb_2O_5–ZrO_2–SiO_2 glass ceramic as follows [42]:

$$g_{\parallel} = 2.0023\left[1 - \frac{4\lambda\alpha^2\beta_1^2}{E(^2B_{2g})}\right] \quad (3)$$

$$g_{\perp} = 2.0023\left[1 - \frac{\lambda\alpha^2\beta^2}{E(^2E_g)}\right] \quad (4)$$

In Eqs. (3) and (4) λ is the spin–orbit coupling coefficient, α^2 is the bonding coefficient due to covalency of the σ bonds with the equatorial ligands that measures the electron density delocalized on ligand ions, β_1^2 accounts for the covalency of π bonding between ligands and $^2B_{2g}$ excited state and β^2 ($\sim$1.00).

The limiting values of bonding parameters α^2 and β_1^2 are 0.5 (pure covalent) and 1 (pure ionic) respectively. The values of α^2 and β_1^2 (Table 6) for the studied samples indicate an increasing tendency towards 1.0 with increase in the concentration of CuO up to 0.2 mol%. This tendency indicates a gradual adaptation of Cu^{2+} ions towards ionic environment. The decrease in the value of bonding parameters (or their approachability towards 0.5) suggests the deviation of copper ions from ionic towards covalent environment. Further, the observed decrease in the intensity of ESR signal of the samples C_{25} and C_{30} suggests the change in the Cu^{2+}/Cu_{tot} ratio to be one of the reasons. Additionally, in the glass ceramic samples the jumping frequency of the charge carriers ($Cu^{+} \rightarrow Cu^{2+}$) is proportional to $\exp(-W/kT)$ [36], where $W = 1/2\ W_D + W_H$; in this, W_D is the mean energy difference between adjacent copper ion sites due to the disordered nature of the glass ceramic and W_H is the activation energy for the hopping process of the polarons between two identical sites. In the case of samples containing higher content of CuO, it is possible to suppose that the leading term is W_H, and that the jumping rate of the polaron is high; this fact, together with the relatively low concentration of the paramagnetic species accounts for the weak ESR signal observed for the samples C_{25} and C_{30}.

In the IR and Raman spectra a gradual increase in the intensity of all Si–O–Si asymmetrical bands and also NbO_6 structural units is observed with increase in the concentration of CuO up to 0.2 mol%. This indicates an increasing degree of disorder in the glass network. In other words, in this concentration range (0–0.2 mol%) the copper ions act as modifiers and depolymerize glass network. The growing intensity of symmetrical bands at the expense of asymmetrical bands in the spectra of the samples containing more than 0.2 mol% of CuO suggests that the copper ions do participate in the network forming with CuO_4 structural units and alternate with SiO_4, ZrO_4 units.

Under the application of high dc field, the electrical forces form orientational field which align the corresponding state dipole moments and form the macroscopic non-centrosymmetry. The coupling of this acentric field with the third order susceptibility, χ^3, gives rise to effective second-order susceptibility through the equation:

$$\chi^{(2)} = 3\chi^{(3)}E_{dc} \quad (5)$$

The induced polarizability is quadratically dependent on the pump electromagnetic wave and the induced coefficient is an effective optical second order nonlinear coefficient $\chi^{(2)}$. This one is commonly believed to arise from the symmetry breaking recorded dc-electric field acting on the third-order nonlinear susceptibility as per Eq. (5). In the present investigation we have observed the highest value of $\chi^{(2)}$; incidentally we have observed the lowest optical band gap for Li_2O–Nb_2O_5–ZrO_2–SiO_2 glasses crystallized with 0.2 mol% of CuO. From the XRD data and even from ESR data we have observed that a considerable proportion of copper ions do exist in Cu^{3+} state

and form $LiCuO_2$ crystal phases. Such phases seemed to be a hindrance for the growth of $\chi^{(2)}$ value and are responsible for low values of $\chi^{(2)}$ for the samples C_{25} and C_{30}.

The maximal NLO effects for the amorphous samples were observed only after heat treatment at higher temperatures (320 °C). Such an observation suggests that the degree of depolymerization that causes the induced dipole moment is less in the samples.

The values of dielectric parameters viz., ε', tan δ and σ_{ac} at any frequency are found to increase with temperature and activation energy for ac conduction is observed to decrease with increase in the content of nucleating agent CuO up to 0.2 mol%; this is an indication of an increase in the space charge polarization. Such an increase is due to the increasing concentration of Cu^{2+} ions that act as modifiers in these samples. These modifying ions generate dangling bonds and non bridging oxygen ions in the glass network. The defects thus produced create easy pathways for the migration of charges that would build up space charge polarization and facilitate an increase in the dielectric parameters as observed [43–45]. The comparatively lower values of these parameters observed for the pre-crystallized samples suggest the lesser degree of disorder in the glass network when compared with that of glass ceramic network.

The value of the effective activation energy associated with the dipoles is observed to decrease with increase in the content of CuO in the glass ceramic network up to 0.2 mol% (Table 6), this observation points out an increasing freedom for dipoles to orient in the field direction, obviously due to increasing degree of disorder in glass ceramic network. The observed dielectric relaxation effects in Li_2O–Nb_2O_5–ZrO_2–SiO_2 glasses crystallized with different concentrations of CuO may be attributed to the association of octahedrally positioned Cu^{2+} ions with a pair of cationic vacancies as observed in a number of conventional glasses, glass ceramics and crystals that contain divalent positive ions as reported before [46,47].

The decrease of the dielectric parameters for the samples mixed with more than 0.2 mol% of CuO obviously suggests the decrease in the concentration of charge carriers responsible for building up space charge polarization. This indirectly supports the viewpoint that the glass ceramic network of the samples C_{25} and C_{30} is more rigid (due to the existence of copper ions in CuO_4 structural units) and contains less proportion of free charge carriers.

The variation of $\log \sigma(\omega)$ *vs.* activation energy for conduction (in the high temperature region) is shown as inset (c) of Fig. 15; the graph yields a near straight line. This observation advocates that the conductivity enhancement is directly related to the thermally stimulated mobility of the charge carriers in the high temperature region. The progressive increase of conductivity with the increase of Cu content up to 0.2 mol% in the glass ceramic is a manifestation of the increasing concentration of mobile electrons, or polarons, involved in the process of transfer from Cu^{2+} to Cu^{3+} ions.

The conductivity at any temperature and frequency as a function of concentration of CuO (Fig. 15) exhibits a maximum at $x = 0.2$ mol%. Though electronic and ionic conductivities are not separated but the observed trend of increase of conductivity and decrease of activation energy for $x < 0.2$ mol% and, decrease of conductivity and increase of activation energy for $x > 0.2$ mol% of CuO content suggests switch over of predominance of conduction mechanism from ionic to electronic [48]. The mobile electrons, or polarons, involved in the process of transfer from $Cu^{2+} \leftrightarrow Cu^{3+}$, are attracted by the oppositely charged cations. This cation–polaron pair moves together as a neutral entity. As expected, the migration of this pair is not associated with any net displacement of the charge and thus does not contribute to electrical conductivity. As a result, we expect a decrease in the conductivity for the samples C_{25} and C_{30}. In other words, with the entry of Cu^{3+} ions into the glass network, the electronic paths are progressively blocked causing an inhibition of the electronic current.

The frequency response of real part of ac conductivity is normally described by power law dependence with s as exponent:

$$\sigma'(\omega) = \sigma_{dc}\left[1 + \left(\frac{\omega}{\omega_c}\right)^s\right], \quad 0 \le s < 1 \tag{6}$$

ω_c is the characteristic macroscopic relaxation frequency.

At short times, when the mean square displacement of ions is small, the ion transport is characterized by the non-random forward–backward hopping process; under these conditions Eq. (6) modifies to

$$\sigma(\omega) \propto \omega^s \tag{7}$$

The variation of the exponent (obtained by plotting $\log \sigma(\omega)$ *vs.* ω) is found to be increasing with the concentration of CuO up to 0.2 mol% (inset (d) of Fig. 15); such an increase suggests an expansion in dimensionality of conducting space with the content of CuO [49,50] up to 0.2 mol% owing to the presence of larger proportions of Cu^{2+} ions in the glass network.

In insulators, where distribution of relaxation times τ exists, as in the present samples, the ac conduction can be represented by

$$\sigma = \sigma_0 e^{-\xi} \tag{8}$$

There are two mechanisms that could contribute to the form of Eq. (7) for ac conduction: the first contribution is due to the normal classical activation of a carrier over a potential barrier '*W*' separating two sites, in this case $\xi = W/kT$. This mechanism can be adapted to the simple Debye loss case. Second contribution is due to the tunneling of a carrier through a potential barrier between the sites separated by a distance R, in this case $\xi = 2\alpha R$, where α^{-1} being the localization strength; this mechanism is applicable for explaining low-temperature part of the conductivity (nearly temperature-independent part). The way the ac conductivity varies with the temperature for the studied glass ceramic samples indicates that both the mechanisms are possible for ac conduction, in Li_2O–Nb_2O_5–ZrO_2–SiO_2:CuO glass ceramics.

Our observations on dielectric parameters of Li_2O–Nb_2O_5–ZrO_2–SiO_2:CuO glass ceramics indicated that the rate of increase of $\varepsilon' \times \tan \delta$ (which is inversely proportional to

dielectric break down strength) with temperature is increasing with increase in the concentration of CuO up to 0.2 mol%. Thus the experiments on dielectric properties of Li_2O–Nb_2O_5–ZrO_2–SiO_2:CuO glasses show a sign of decrease in the dielectric breakdown strength of the glasses with increase in the concentration of CuO up to 0.2 mol% owing to the larger degree of disorder in the glass ceramic network.

5. Conclusions

We have synthesized Li_2O–Nb_2O_5–ZrO_2–SiO_2 glasses and subsequently crystallized them with different concentrations of CuO (0–0.3 mol% in the steps of 0.05) as nucleating agent and characterized. The characterization of the samples by SEM, XRD and DSC techniques have indicated that the samples contain well defined and randomly distributed grains of different crystalline phases. The interesting orthorhombic crystalline phases like LiCuO and $LiCuO_2$ in which the copper ions exist as Cu^+ and Cu^{3+} states were also detected in these samples. The IR and Raman spectral studies have indicated that the glass ceramic samples contain various structural units with the linkages of the type Si–O–Si, Nb–O–Nb, Zr–O–Zr, and Si–O–Zr; the increasing content of CuO in the glass ceramics seemed to have weakened such linkages. The analysis of the results of optical absorption, ESR and photoluminescence spectra of the studied glass ceramics have indicated that a considerable proportion of copper ions do exist in Cu^+ state in addition to Cu^{2+} state especially in the samples crystallized with more than 0.2 mol% CuO. The analysis of the results of dielectric studies has suggested a decrease in the insulating character with increase in the crystallizing agent of these samples up to 0.2 mol% ac conductivity in the high temperature region seems to be connected mainly with the polarons involved in the process of transfer from Cu^+ to Cu^{2+}. Photoinduced second order susceptibility studies (after the samples were dc field treated at elevated temperatures) with 10 ns Er:glass laser (of wavelength 1540 nm with power densities up to 1.5 GW/cm^2) have indicated that 0.2 mol% of CuO is the optimal concentration for getting the highest values of second order susceptibility coefficients.

Acknowledgements

Two of the authors T. Sri Kumar and Ch. Srinivasa Rao wish to thank UGC, Govt. India and the Management of Andhra Loyola College, Vijayawada for sanctioning study leave under FDP.

References

[1] V.N. Sigaev, V.S. Ryzhenkov, S.V. Lotarev, N.V. Golubev, S.Yu. Stefanovich, A. Okada, Glasses and their crystallization in the $(1-x)\,NbO_3{\cdot}x$-SiO_2 system at low glass-forming oxide contents, $0 \leq x \geq 0.35$, J. Non-Cryst. Solids 356 (2010) 958–965.

[2] A.A. Lipovskii, D.K. Tagantsev, A.A. Vetrov, O.V. Yanush, Raman spectroscopy and the origin of electrooptical Kerr phenomenon in niobium alkali-silicate glasses, J. Opt. Mater. 21 (2003) 749–757.

[3] K. Narita, Y. Takahashi, Y. Benino, T. Fujiwara, T. Komatsu, Unique crystallization and formation of nonlinear optical (Na, K)NbO_3 phases in (Na, K)$NbGeO_5$ glasses, Opt. Mater. 259 (2004) 393–400.

[4] M. Miyata, H. Nasu, A. Mito, K. Kurachi, J. Matsuoka, K. Kamiya, Second-harmonic generation from electrically poled niobium alkali silicate glasses, J. Appl. Phys. 34 (1995) 1455–1457.

[5] H. Yang, S. Wu, J. Hu, Z. Wang, R. Wang, H. He, Influence of nano-ZrO_2 additive on the bending strength and fracture toughness of fluoro-silicic mica glass-ceramics, Mater. Des. 32 (2011) 1590–1593.

[6] S. Banijamali, B.E. Yekta, H.R. Rezaie, V.K. Marghussian, Crystallization and sintering characteristics of CaO–Al_2O_3–SiO_2 glasses in the presence of TiO_2, CaF_2 and ZrO_2, Thermochim. Acta 488 (2009) 60–65.

[7] E.M.M. Ewais, M.A.A. Attia, A. Abousree-Hegazy, R.K. Bordia, Investigation of the effect of ZrO_2 and ZrO_2/Al_2O_3 additions on the hot-pressing and properties of equimolecular mixtures of α- and β-Si_3N_4, Ceram. Int. 36 (2010) 1327–1338.

[8] A. Sawa, K. Nakanishi, T. Hanada, Preparation and properties of radio-frequency sputtered X-ray amorphous films in the system SiO_2–ZrO_2, Thin Solid Films 516 (2008) 4665–4672.

[9] D. Tauch, C. Rüssel, Glass-ceramics in the system $BaO/TiO_2(ZrO_2)/Al_2O_3/B_2O_3$ and their thermal expansion, J. Non-Cryst. Solids 353 (2007) 2109–2114.

[10] T. Komatsu, K. Koshiba, T. Honma, Preferential growth orientation of laser-patterned $LiNbO_3$ crystals in lithium niobium silicate glass, J. Solid State Chem. 184 (2011) 411–418.

[11] L.R. Pinckney, Transparent high strain point spinal glass-ceramics, J. Non-Cryst. Solids 255 (1999) 171–177.

[12] G.H. Beall, L.R. Pinckney, Nanophase glass-ceramics, J. Am. Ceram. Soc. 82 (1999) 5–16.

[13] I.V. Kityk, B. Marciniak, B. Sahraoui, Photoinduced electrooptics in pyrene molecular crystallites incorporated within polymer matrices, Cryst. Res. Technol. 37 (2002) 477–484.

[14] S. Tkaczyk, M. Galceran, S. Kret, M.C. Pujol, M. Aguilo, F. Diaz, A.H. Reshak, I.V. Kityk, UV-excited piezo-optical effects in oxide nanocrystals incorporated into PMMA matrices, Acta Mater. 56 (2008) 5677–5684.

[15] M. Williams, D. Hunter, A.K. Pradhan, I.V. Kityk, Photoinduced piezo-optical effect in Er doped ZnO films, Appl. Phys. Lett. 89 (2006) 043116.

[16] T. Miura, T. Watanabe, Y. Benino, T. Komatsu, R. Sato, Unusual elastic and mechanical behaviors of copper phosphate glasses with different copper valence states, J. Am. Ceram. Soc. 84 (2001) 2401–2408.

[17] E. Cattaruzza, G. Battaglin, F. Gonella, R. Polloni, B.F. Scremin, G. Mattei, P. Mazzoldi, C. Sada, Au–Cu nanoparticles in silica glass as composite material for photonic applications, Appl. Surf. Sci. 254 (2007) 1017–1021.

[18] B. Karthikeyan, M. Anija, C.S. Suchand Sandeep, T.M. Muhammad Nadeer, Reji Philip, Optical and nonlinear optical properties of copper nanocomposite glasses annealed near the glass softening temperature, Opt. Commun. 281 (2008) 2933–2937.

[19] R. Kibar, A. Çetin, N. Can, Effect of thermal treatment on linear optical properties of Cu nanoclusters, Physica B 404 (2009) 105–110.

[20] J. Sheng, S. Chen, J. Zhang, Li Juan, J. Yu, UV-light irradiation induced copper nanoclusters in a silicate glass, Int. J. Hydrogen Energy 34 (2009) 1119–1122.

[21] M. Winter, J.O. Besenhard, M.E. Spahr, P. Novák, Insertion electrode materials for rechargeable lithium batteries, Adv. Mater. 10 (1998) 725–763.

[22] M.R. Poulsen, P.I. Borel, J. Fage-Pedersen, J. Hübner, M. Kristensen, J.H. Povlsen, K. Rottwitt, M. Svalgaard, W.E. Svendsen, Advances in silica-based integrated optics, Opt. Eng. 42 (2003) 2821.

[23] M.K. Balakirev, I.V. Kityk, V.A. Smirnov, L.I. Vostrikova, J. Ebothe, Anisotropy of the optical poling of glass, Phys. Rev. A67 (2003) 023806.

[24] Powder Diffraction File, Alphabetical Index, Inorganic Compounds, JCPDS, International Centre for Diffraction Data, Newtown Square, PA 19073-3273, 2003.

[25] K. Imai, M. Koike, H. Takei, H. Sawa, D. Shiomi, K. Nozawa, M. Kinoshita, Preparation, crystal structure and magnetic property of a new compound $LiCuO_2$, J. Phys. Soc. Jpn. 61 (1992) 1819–1820.

[26] M. Nakamura, Y. Mochizuki, K. Usami, Y. Itoh, T. Nozaki, Infrared absorption spectra and compositions of evaporated silicon oxides (SiO_x), Solid State Commun. 50 (1984) 1079–1081.

[27] Y. Yu, X. Wang, Y. Cao, X. Hu, Study on the structure and properties of ZrO_2 buffer layers on stainless steel by XRD, IR and AES, Appl. Surf. Sci. 172 (2001) 260–264.
[28] K.J. Rao, Structural Chemistry of Glasses, Elsevier, Amsterdam, 2002.
[29] U. Selvaraj, K.J. Rao, Role of lead in lead phosphomolybdate glasses and a model of structural units, J. Non-Cryst. Solids 104 (1988) 300–315.
[30] I. Ardelean, S. Cora, V. Ioncu, Structural investigation of $CuO–Bi_2O_3–B_2O_3$ glasses by FT-IR, Raman and UV–VIS spectroscopies, J. Optoelectron. Adv. Mater. 8 (2006) 1843–1847.
[31] V.H. Klassen, R. Hopper, Die $K_4[Ag_4O_4]$–Strukturfamilie, Z. Anorg. Allg. Chem. 486 (1982) 101–114.
[32] K. Nakamura, T. Moriga, A. Sumi, Y. Kashu, Y. Michihiro, I. Nakabayashi, T. Kanashiro, NMR study on the Li^+ ion diffusion in $LiCuO_2$ with layered structure, Solid State Ionics 176 (2005) 837–840.
[33] K. Tanaka, Glass transition of covalent glasses, Solid State Commun. 54 (1985) 867–869.
[34] F. Branda, A. Buri, A. Marotta, S. Saiello, Kinetics of crystal growth in $Na_2O{\cdot}2SiO_2$ glass. A DTA study, Thermochim. Acta 77 (1984) 13–18.
[35] S.V.G.V.A. Prasad, G. Sahaya Baskaran, N. Veeraiah, Spectroscopic, magnetic and dielectric investigations of $BaO–Ga_2O_3–P_2O_5$ glasses doped by Cu ions, Phys. Stat. Solidi A 202 (2005) 2812–2828.
[36] B. Di Bartolo (Ed.), Spectroscopy of Solid-State Laser-Type Materials, Plenum Publishing Corporation, New York, 1987, p. 238.
[37] A.A. Kaminskii, Laser Crystals, 2nd ed., Springer, Berlin, 1989.
[38] Y. Fujimoto, M. Nakatsuka, Spectroscopic properties and quantum yield of Cu-doped SiO_2 glass, J. Lumin. 75 (1997) 213.
[39] K. Fukumi, A. Chayahara, K. Ohora, N. Kitamura, Y. Horino, K. Fujii, M. Makihara, J. Hayakaya, N. Ohno, Photoluminescence of Cu^+-doped silica glass prepared by MeV ion implantation, Nucl. Instrum. Methods B 149 (1999) 77.
[40] I. Ardelean, M. Peteanu, V. Simon, O. Cozar, F. Ciorcas, S. Lupsor, Structural and magnetic properties of $CuO–TeO_2–B_2O_3–SrO$ glasses, J. Magn. Magn. Mater. 196 (1999) 253–254.
[41] L. Srinivasa Rao, M. Srinivasa Reddy, D. Krishna Rao, N. Veeraiah, Influence of redox behavior of copper ions on dielectric and spectroscopic properties of $Li_2O–MoO_3–B_2O_3$:CuO glass system, Solid State Sci. 11 (2009) 578–587.
[42] E. Metwalli, Copper redox behavior, structure and properties of copper lead borate glasses, J. Non-Cryst. Solids 317 (2003) 221–230.
[43] G. Sahaya Baskaran, M.V. Ramana Reddy, D. Krishna Rao, N. Veeraiah, Dielectric properties of $PbO–P_2O_5–As_2O_3$ glass system with Ga_2O_3 as additive, Solid State Commun. 145 (2008) 401–406.
[44] T. Sankarappa, M. Prashant Kumar, G.B. Devidas, N. Nagaraja, R. Ramakrishnareddy, AC conductivity and dielectric studies in $V_2O_5–TeO_2$ and $V_2O_5–CoO–TeO_2$ glasses, J. Mol. Struct. 889 (2008) 308–315.
[45] G. Murali Krishna, B. Anila Kumari, M. Srinivasa Reddy, N. Veeraiah, Characterization and physical properties of $Li_2O–CaF_2–P_2O_5$ glass ceramics with Cr_2O_3 as a nucleating agent, J. Solid State Chem. 180 (2007) 2747–2755.
[46] T. Srikumar, Ch. Srinvasa Rao, Y. Gandhi, N. Venkatramaiah, V. Ravikumar, N. Veeraiah, Microstructural, dielectric and spectroscopic properties of $Li_2O–Nb_2O_5–ZrO_2–SiO_2$ glass system crystallized with V_2O_5, J. Phys. Chem. Solids 72 (2011) 190–200.
[47] Y. Gandhi, N. Krishna Mohan, N. Veeraiah, Role of nickel ion coordination on spectroscopic and dielectric properties of $ZnF_2–As_2O_3–TeO_2$:NiO glass system, J. Non-Cryst. Solids 357 (2011) 1193–1202.
[48] R.A. Montani, M.A. Frechero, The conductive behaviour of silver vanadium–molybdenum tellurite glasses, Solid State Ionics 158 (2003) 327–332.
[49] D.L. Sidebottom, Dimensionality dependence of the conductivity dispersion in ionic materials, Phys. Rev. Lett. 83 (1999) 983–998.
[50] S. Bhattacharya, A. Ghosh, Conductivity spectra in fast ion conducting glasses: mobile ions contributing to transport process, Phys. Rev. B 70 (2004) 172203.